Localization and phosphorylation in the Snf1 network is controlled by two independent pathways

Niek Welkenhuysen[1,2, †], Linnea Österberg[1,2, †], Sebastian Persson[2], Stefan Hohmann[1], Marija Cvijovic[2*]

[1]Department of Biology and Biological Engineering, Chalmers University of Technology, Sweden

[2]Department of Mathematical Sciences, Chalmers University of Technology and University of Gothenburg, Sweden

†Authors contributed equally

*Corresponding author:
Marija Cvijovic
Department of Mathematical Sciences,
Chalmers University of Technology and University of Gothenburg
SE-412 96 Gothenburg
Sweden

marija.cvijovic@chalmers.se
+46317725321

Abstract:

AMPK/SNF1 is the master regulator of energy homeostasis in eukaryotic cells and has a key role in glucose de-repression. If glucose becomes depleted, Snf1 is phosphorylated and activated. Activation of Snf1 is required but is not sufficient for mediating glucose de-repression indicating a second glucose-regulated step that adjusts the Snf1 pathway. To elucidate this regulation, we further explore the spatial dynamics of Snf1 and Mig1 and how they are controlled by concentrations of hexose sugars. We utilize fluorescence recovery after photobleaching (FRAP) to study the movement of Snf1 and how it responds to external glucose concentrations. We show that the Snf1 pathway reacts both to the presence and to the absolute concentration of glucose. Furthermore, we identify a negative feedback loop regulating Snf1 activity. We also show that Mig1 localization correlates with the Snf1 phosphorylation pattern and not with the Mig1 phosphorylation pattern, suggesting that inactivation of Snf1 has a more pronounced effect on the localization of Mig1 than on the phosphorylation of Mig1. Our data offer insight into the true complexity of regulation of this central signaling pathway by one signal (glucose depletion) interpreted by the cell in different ways.

Introduction

AMPK and its yeast homolog SNF1 is the master regulator of energy homeostasis in eukaryotic cells (Hardie, 2014; Hardie et al., 2012). The AMPK/SNF1 family of protein kinases is regulated by multiple stimuli that signal an energy depletion or a significant rise in energy demand. In the yeast *Saccharomyces cerevisiae* the primary function of SNF1 is adaptation to glucose limitation when the use of alternative carbons sources is needed to achieve growth and proliferation (Hedbacker and Carlson, 2008). In addition, a broad spectrum of downstream effects, such as lipid biogenesis and gluconeogenesis, is affected by the SNF1 pathway to balance the energy demand and supply (Usaite et al., 2009; Zhang et al., 2010).

The Snf1 kinase is constitutively activated by three upstream kinases Elm1, Sak1 and Tos3 (García-Salcedo et al., 2014; Hong et al., 2003; Nath et al., 2003). When a high energy-yield sugar becomes available, such as the hexose sugars glucose, fructose or mannose, Snf1 is rapidly dephosphorylated by the PP1 phosphatase Reg1/2-Glc7, Sit4 or Ptc2 (Ruiz et al., 2013, 2011; Zhang et al., 2011). The catalytic unit Snf1 alone is not sufficient to mediate glucose de-repression. For stable Snf1 activity, two more proteins need to bind Snf1 to form the heterotrimeric kinase complex SNF1 (Celenza et al., 1989; Schmidt and McCartney, 2000). The SNF1 complex consists of the catalytic alpha-subunit Snf1, regulatory gamma-subunit Snf4 and a beta-subunit, which can either be Gal83, Sip1 or Sip2 (Jiang and Carlson, 1997; Schmidt and McCartney, 2000). The binding of ADP to Snf4 protects from dephosphorylation and inactivation of Snf1 (Chandrashekarappa et al., 2013; Mayer et al., 2011). ATP competes with ADP for these binding sites, and this competition functions as an energy sensor (Mayer et al., 2011). The subcellular localization of the complex is regulated by the beta-subunits (Vincent et al., 2001). Localization studies of the three isoforms under high glucose conditions showed that all the beta-subunits seem to reside in the cytosol. With ethanol as the sole energy source, the Sip1 isoform is associated with the vacuolar membrane. Sip2 is located in the cytoplasmic, and Gal83 accumulates in the nucleus (Chandrashekarappa et al., 2016; Vincent et al., 2001). Under the shift from high glucose concentrations to ethanol as the sole carbon source, a major proportion of Snf1 and Snf4 localizes together with Gal83 to the nucleus (Vincent et al., 2001).

Active Snf1 changes gene expression enabling the cell to employ alternative carbon sources (Gancedo, 1998). To alter gene transcription in the cell, Snf1 phosphorylates several transcription factors, among which Mig1 is the most prominent (Ostling and Ronne, 1998; Treitel et al., 1998). Mig1 in the unphosphorylated state represses genes required for the utilization of alternative carbon sources. Phosphorylated Mig1 relocates to the nucleus and interacts with Cyc8/Ssn6 and Tup1 to repress transcription of glucose repressed genes (Keleher et al., 1992; Treitel and Carlson, 1995). When the primary energy sources are depleted, Snf1 phosphorylates Mig1 on at least four sites (DeVit and Johnston, 1999; Treitel et al., 1998). This leads to Mig1 exiting the nucleus (DeVit and Johnston, 1999). This relocation of Mig1 results in the alleviation of glucose repression and allows the expression of genes such as *SUC2* and *HXK1*, which are required for the use of alternative carbon sources (Carlson et al., 1981; Lutfiyya et al., 1998; Lutfiyya and Johnston, 1996; Treitel et al., 1998). Therefore, Mig1 is commonly used as a readout for the Snf1/Mig1 pathway. The dynamics of Mig1 relocation in response to different concentrations of hexoses has been studied before and is established as a measurement for the SNF1 pathway activity (Bendrioua et al., 2014; Schmidt et al., 2020; Welkenhuysen et al., 2017; Wollman et al., 2017). FRAP studies on Mig1 have shown nucleocytoplasmic shuttling, regardless of the external glucose concentrations (Bendrioua et al., 2014). The Mig1 protein pool follows a double exponential kinetic profile, indicating two different fractions of the protein pool that follow different kinetic patterns. The rates of the

protein pool depend on the glucose concentration (Bendrioua et al., 2014; Wollman et al., 2017).

Activation of SNF1 is required but is not sufficient for mediating glucose de-repression. Overexpression of Sak1 or addition of sodium and lithium ions leads to activation of Snf1, but not to glucose de-repression (García-Salcedo et al., 2014; Ye et al., 2008). This indicates that a second glucose-regulated step governs the Snf1/Mig1 pathway activity (García-Salcedo et al., 2014). How Snf1 is regulated in this second step after activation is unknown. To better understand this regulatory step, we further explore the spatial dynamics of the Snf1 and Mig1 and how they are controlled by concentrations of hexose sugars. We utilize fluorescence recovery after photobleaching (FRAP) to study the movement of Snf1 and how it responds to external glucose concentrations. We show that the Snf1 pathway reacts both to the presence as well as to the absolute concentration of glucose. We identify a negative feedback loop regulating Snf1 activity, as well as distinct kinetic behaviors in Snf1 nucleocytoplasmic shuttling that are dependent on both carbon source and concentration.

Results

The kinetics of Snf1 nucleocytoplasmic shuttling is driven by carbon source availability

It is unclear how the Snf1 dynamic spatial distribution contributes to Snf1's role in the glucose derepressing pathway. To further understand how Snf1 mechanistically regulates energy balance in the cell, we employed fluorescence recovery after photobleaching (FRAP). Exponentially grown yeast cells with a Snf1-GFP construct were exposed to YNB under three different conditions: 2% glucose, 0.05% glucose or 2% glycerol for at least 1.5 h before the onset of the experiment. The fluorescent Snf1 in the nucleus is bleached, and the subsequent recovery of fluorescence in the nucleus is observed. The FRAP data were analyzed with a non-linear mixed effect framework (NLME), assuming both a single (Figure 1) and a double (SI data files 2, 3 and 4) exponential model. Non-linear mixed-effects modelling is typically used for longitudinal data exhibiting both within and between-subject variability (Davidian and Giltinan, 2003). This method has been widely used in pharmacokinetics and pharmacodynamic studies (Lavielle and Mentré, 2007; Sissoko et al., 2016), but in recent years it is exploited in single-cell time-lapse data facilitating our understanding of cell-to-cell variability (Almquist et al., 2015; Llamosi et al., 2016; Welkenhuysen et al.,; 2017 Persson et al., 2020). When analyzing fluorescence measurements of a tagged protein in single cells over time, the observed intensity will differ between measurements even if the cells are in a steady-state due to the measurement error. Moreover, owing to extrinsic variability, cells will have different intensity levels. Using a mixed-effects framework, the observed cell-to-cell variability can be accounted for in the analysis by letting the rate parameters vary between cells according to a probability distribution. Furthermore, a mixed-effects framework allows the assessment of potential correlations between parameters in different cells.

Both single and double models were able to describe the data well. However, the Fisher matrix indicates overfitting when using the double exponential equation (summary statistics in SI data files 2, 3 and 4 and complete results at https://github.com/cvijoviclab/Mig1_frap_nlme). The single exponential fit performed best for all conditions (Figure 1A). The 0.05% glucose showed slightly inconsistent behavior with a single exponential curve, but the analysis of the model diagnostics shows that a single-exponential model gives a good approximation of the kinetic behavior.

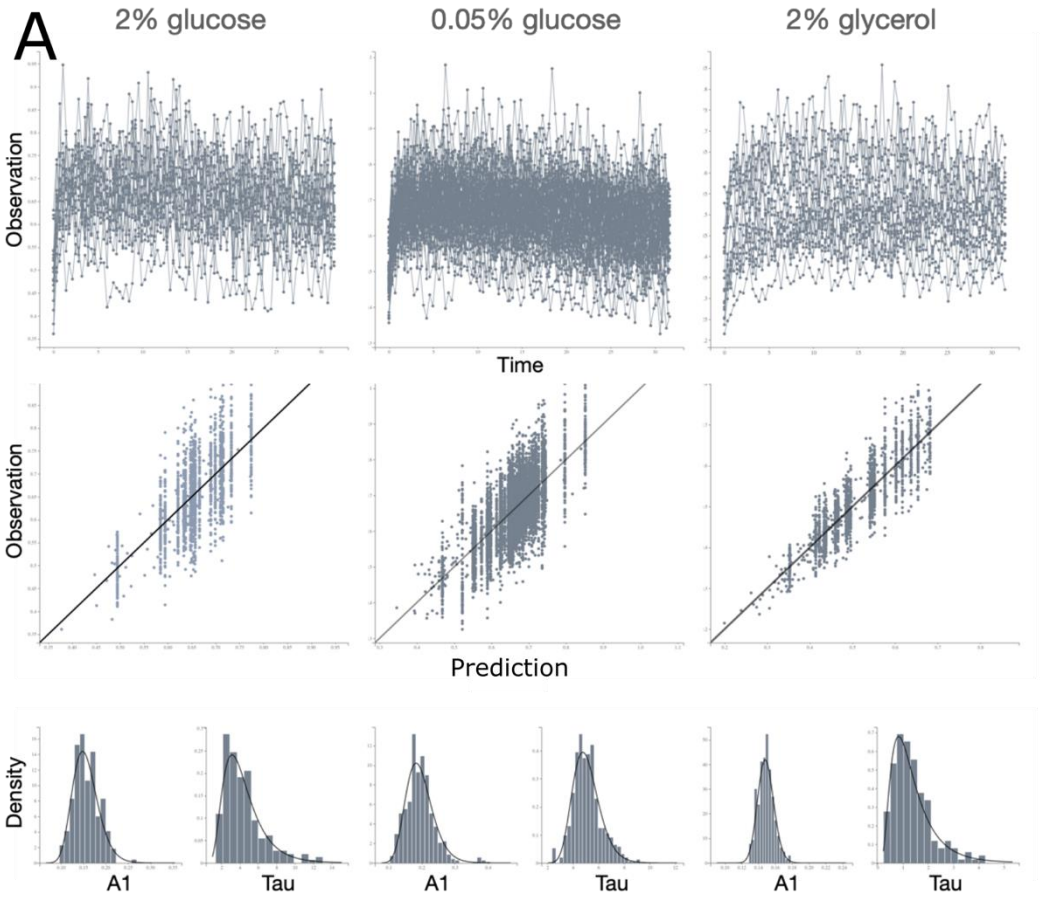

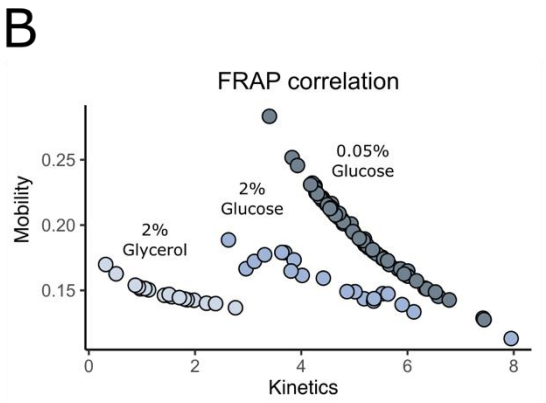

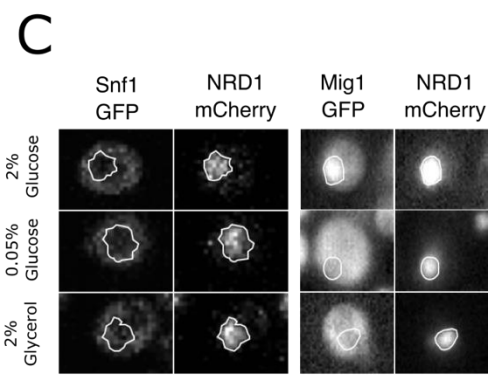

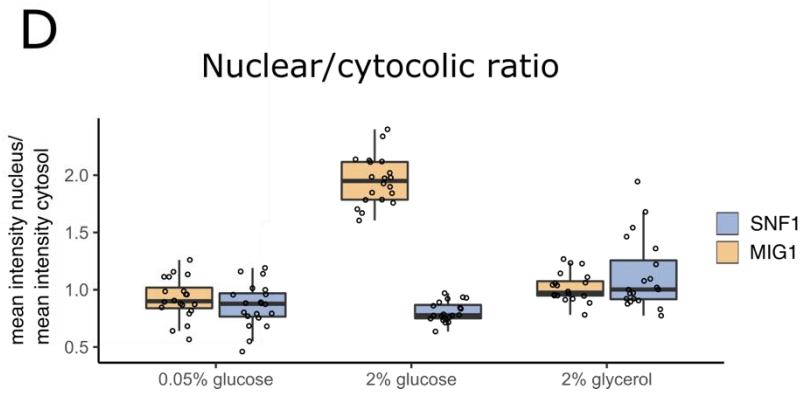

Figure 1: FRAP (Snf1) and nuclear localization (Snf1 and Mig1) measurements of exponentially grown cells exposed to YNB with either 2% glucose, 0.05% glucose or 2% glycerol. (A) the single-cell recovery curves from the FRAP experiment, individual prediction versus observation (IPRED) plot based on the single exponential fit ($I = I_0 + A1 * (1 - e^{-tau1*t})$, I_0 represents the degree of bleaching), and the resulting marginal density plots for both the individual parameters (bar) and population distributions (line) for the parameters $A1$ (the mobility constant) and $tau1$ (the kinetic constant). (B) the correlation between the individual parameters. (C) Snf1-GFP and Mig1-GFP fluorescence relative to the nuclear marker Nrd1-mCherry. The nuclear-to-cytosolic ratio (NC ratio) was calculated by dividing the mean of the fluorescence in the nucleus with the mean of the fluorescence in the cytosol. (D) single-cell nuclear-to-cytoplasmic ratio of Snf1 and Mig1.

The fluorescently tagged Snf1 was significantly bleached during the FRAP experiment, and the nuclear fractions differ between conditions, hence the mobility (parameter $A1$) did not accurately reflect the mobile fraction. To correct for the bleached population, we used the steady-state value of the nuclear fraction and the estimated degree of bleaching in each condition (I_0) to calculate the mobile and immobile fractions of Snf1 (Table 1). The Snf1 steady-state nuclear fractions were similar in high and low glucose (Figure 1D), the mean fold change of 1.06 when comparing 0.05% glucose to 2% glucose, were not significant (p-value = 0.5479). At 2% glycerol the mean NC ratio was increased with a fold change of 1.39 relative 2% glucose (p-value = 1e-05) and 1.30 compared to 0.05% glucose (p-value = 0.0072). The localization of Snf1 seems to be more sensitive to the type of carbon source than the level of glucose which is clear when measuring the nuclear localization of the Snf1 target Mig1. Mig1 has a 2.20-fold decrease when comparing the mean NC ratio of 0.05% to 2% glucose (p-value = 4.4e-11) and a 1.98-fold decrease when comparing 2% glycerol to 2% glucose (p-value = 4.4e-11). There was no significant difference of Mig1 nuclear localization between 0.05% glucose and 2% glycerol (p-value = 0.23). This indicates that Snf1 nuclear localization is primarily controlled by carbon source, that the relative difference in glucose concentration has a smaller effect than the carbon source itself compared to its target Mig1. Unlike Snf1, Mig1 nuclear localization is more affected by a change in glucose level than the change to a less favorable carbon source. This is also reflected in the kinetic coefficient for Snf1 where the cells grown in glucose show a fast nuclear-cytoplasmic shuttling, in contrast to the cells grown in glycerol showing a slow nuclear-cytoplasmic shuttling (Table 1).

Table 1: FRAP population parameters for Snf1 separated by the fixed effects and standard deviation of random effects (W). Correlation between the kinetic constant (tau1) and mobility (A1), the degree of bleaching (I_0) as well as steady-state data and calculated fractions.

	2% glucose		**0.05% glucose**		**2% glycerol**	
	Y_p	S.E	Y_p	S.E	Y_p	S.E
$A1$	**0.153**	0.0177	**0.191**	0.00804	**0.149**	0.0157
$tau1$	**3.93**	0.961	**4.98**	0.18	**1.18**	0.221
I_0	**0.501**	0.0201	**0.464**	0.00839	**0.358**	0.0245
W_{A1}	**0.184**	0.108	**0.209**	0.0252	**0.0642**	0.0464
W_{tau1}	**0.471**	0.22	**0.207**	0.0255	**0.592**	0.139
W_{I_0}	**0.104**	0.0205	**0.108**	0.011	**0.25**	0.0406

corr A1-tau1	**-0.715**	0.432	**-0.998**	0.00175	**-0.917**	0.322
I_{nuc}/I_{cyt}	**0.813**	0.00424	**0.856**	0.00494	**1.117**	0.00580
Mobile fraction	**0.897**		**0.9224**		**0.872**	
Immobile fraction	**0.103**		**0.0776**		**0.128**	

The NLME regression approach provides information about cell-to-cell variability and the correlation between population parameters. We observed a strong negative correlation between mobility and the kinetic coefficient (Table 1 and Figure 1B), where cells with a high mobile fraction show a slower kinetic behavior. The opposite relationship was observed between conditions (Figure 1B), where cells grown in 0.05% glucose, with an overall higher mobile fraction, have a general faster kinetic behavior. In this aspect, the carbon source seems to have a different role than the glucose concentration since the immobile fraction decreases with decreasing glucose levels but increases with a less favorable carbon source.

Snf1 phosphorylation status correlates with Mig1 localization but not with the phosphorylation status

The FRAP experiments showed that Snf1 localization and nucleocytoplasmic shuttling parameters show a larger difference depending on the type of carbon source than on the energy levels. We set out to find if this relationship is also present in the phosphorylation pattern of Snf1 and Mig1. Samples were taken three minutes after a carbon-source concentration change and analyzed by Western blot. The concentration shift was performed from ethanol as carbon source to a glucose concentration of 0%, 0.05%, 0.2%, 0.5%, 1%, and 4%. Dephosphorylation of Snf1 is measured with an antibody that recognizes the phosphorylated form of Snf1 (see Material and Methods). A change in phosphorylation status occurred at all glucose concentrations upshifts. A significant difference (paired student t-test $p<0.001$) between the 0% and 0.05% and 1% was observed (Figure 2A and Figure S1A). This suggests that the bulk of Snf1 protein in the cell is dephosphorylated as soon glucose is taken up by the cell. Phosphorylated Mig1 has a different migration pattern than non-phosphorylated Mig1 and, therefore, can be separated through Western blot. In a lower glucose concentration, Mig1 shows the same migration pattern as at the 0% glucose (Figure 2B and Figure S1B). Only at concentrations higher than 0.5%, a non-phosphorylated species is observed. The significant difference between 0% and 0.05% compared to the upshift to 4% was confirmed with a paired student t-test with a p-value of $p<0.015$ for 0% and $p<0.005$ for 0.05%.

The initial short-term phosphorylation status of Snf1 and Mig1 showed a considerable difference. Snf1 is dephosphorylated as soon as the cell is exposed to 0.05% glucose, while dephosphorylated Mig1 can only be observed at concentrations higher than 0.5%. As the Mig1 nuclear localization is used as a measurement for SNF1 pathway activity, we monitored the nuclear localization of Mig1 to determine if it correlates with the Snf1 or Mig1 phosphorylation pattern. Mig1 readily localized to the nucleus after exposure to both low and high concentration of glucose (Figure 2C, Figure S1C).

Next, we studied the expression of genes under the conditions tested above. As a measure for *HXK1* and *SUC2* gene expression, we utilized a plasmid expressing rapidly degradable YFP from either the *HXK1* or *SUC2* promotor (Schmidt et al., 2020). We only observed an expression from the *HXK1* and *SUC2* promotor at 0.05% glucose, while no notable increase in expression was observed at 0% and 4% glucose (Figure 2D). The nuclear Mig1 observed at 0.05% is only temporary; after an initial nuclear localization, the nuclear signal of Mig1 declines (SI Figure 1).

Overall, we show that in cells exposed to 0% glucose, Snf1 and Mig1 are initially phosphorylated, and Mig1 resides in the cytosol. At 0.05% glucose Snf1 becomes dephosphorylated, while Mig1 remains phosphorylated but partially enters the nucleus. Finally, at 4% glucose, both Mig1 and Snf1 are in the non-phosphorylated form, and Mig1 is in the nucleus (Figure 2).

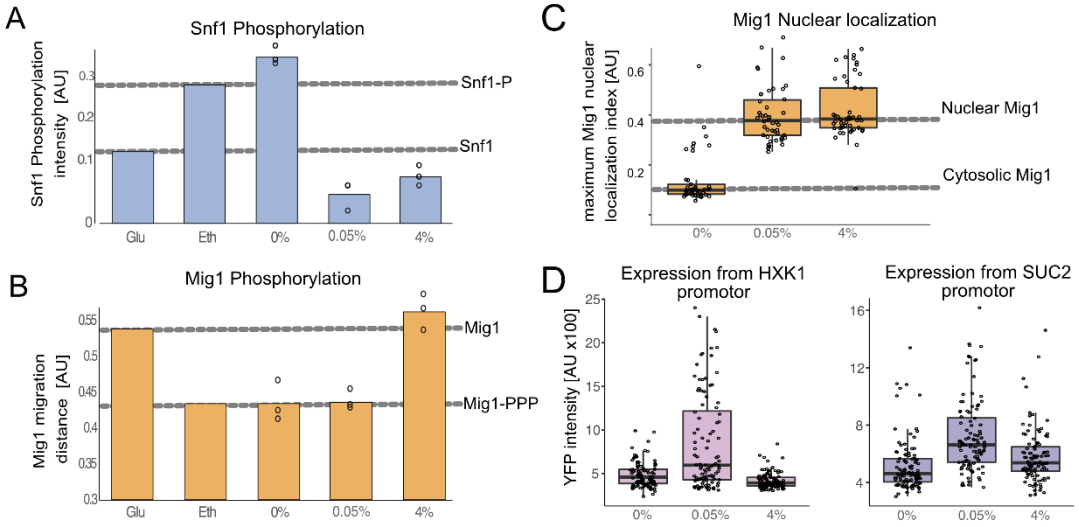

Figure 2: Cells were exposed to upshift (3 min) to higher glucose concentrations (0%, 0.05% and 4%). Glucose and ethanol represent Snf1 phosphorylation intensity in steady-state conditions. (A) Snf1 phosphorylation and (B) Mig1 phosphorylation as measured by Western blot from three independent experiments. The horizontal dotted gray lines represent the intensity in the steady-state conditions. (C) the maximum Mig1 nuclear localization in wild type cells within 15 minutes after the shift from ethanol to the indicated glucose concentration (0%, 0.05% and 4%). The horizontal dotted gray lines represent the localization index indicating (bulk) Mig1 located in the nucleus or cytosol. (D) the level of expression from the *HXK1* and *SUC2* promotors. Fluorescence intensity of YFP expressed through the *HXK1* or *SUC2* promotor after two hours shift to 0%, 0.05% and 4%.

The short-term Mig1 response is more sensitive to glucose than to fructose and mannose

To better understand the sensitivity of the initial Snf1/Mig1 pathway response towards different carbon source levels, cells were exposed to glucose, mannose and fructose. Through fluorescent time-lapse microscopy, the initial spatial response of Mig1 was observed. We exposed cells to concentration shifts from ethanol to 0%, 0.005, 0.05%, 0.5%, 1%, and 4% glucose, mannose or fructose. Mig1 localizing to the nucleus has been observed at 0.005% glucose. While in upshift to mannose and fructose (Figure 3 and Figure S2), Mig1 nuclear

localization was only observed at concentrations above 0.05%. These results suggest that the Mig1 nuclear import is more sensitive to glucose than to mannose and fructose. For the upshift to mannose, the maximum nuclear intensity was already reached at the upshift to 0.05% glucose, and the average nuclear intensity did not increase more. Glucose reaches a maximum Mig1 nuclear intensity at a lower concentration compared to fructose. This could be a consequence of the import rates of these hexose sugars since the maximum import rate of glucose is lower than the import rate of fructose (Berthels et al., 2008). Altogether, this suggests that the nuclear import rate of Mig1 is coupled to the import of Mig1 in the cell or the availability of the hexose sugars inside the cell. Overall, for all hexoses, the Mig1 nuclear intensity increased in a dose-dependent manner, with the rate of increase being hexose specific.

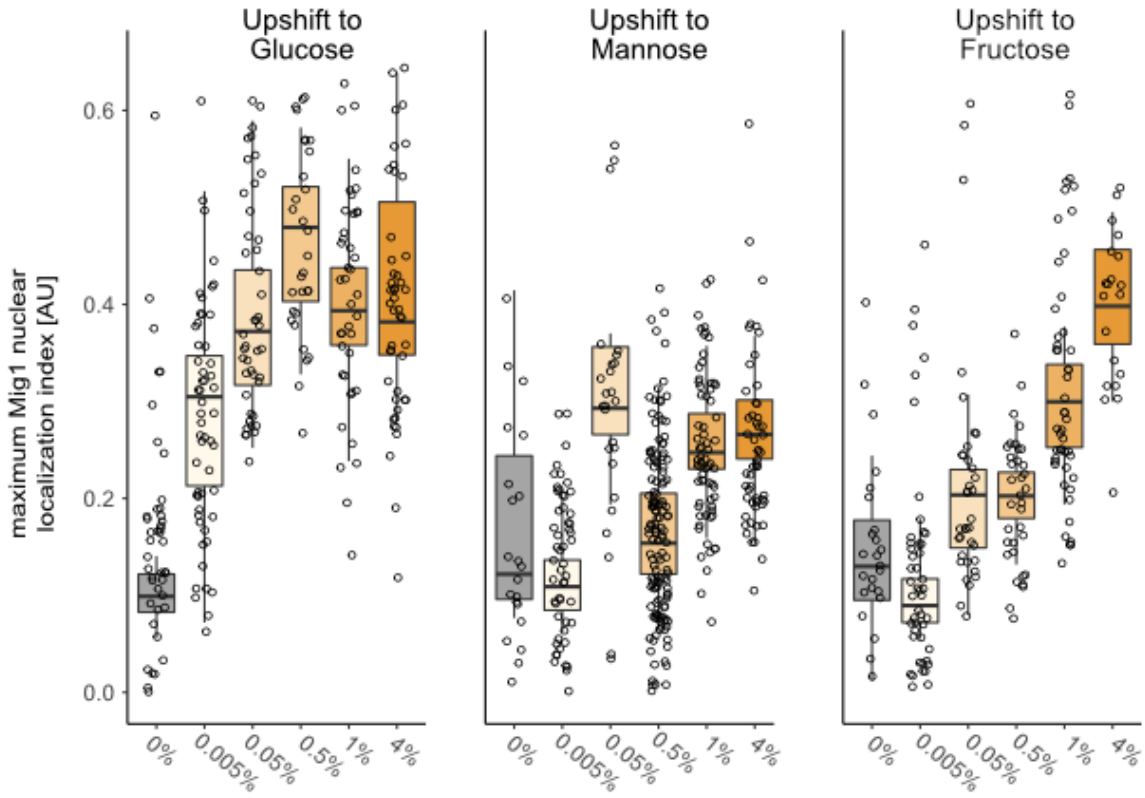

Figure 3: Mig1 nuclear localization in cells after the shift from ethanol to the indicated concentration of glucose, mannose or fructose. Mig1 localization within the observation time of 15 minutes. Each circle represents the maximum Mig1 localization for one cell. Horizontal lines indicate the mean, the boxplot has as lower and upper hinge respectively the 25th and 75th percentile and the whiskers denote the 95% confidence interval. The horizontal dotted gray lines represent either localization index which indicates (bulk) Mig1 located in the nucleus, or cytosol.

Materials & Methods

Strains and plasmids

Yeast strains were grown at 30◦C in YNB synthetic complete medium containing 1.7 g/l yeast nitrogen base, 5 g/l ammonium sulfate, 670 mg/l complete supplement mix with appropriate drop out where applicable; supplemented with carbon source as indicated by the specific experiments.

Strains used in this study:

BY4741 *MATa his3Δ1 leu2Δ0 met15Δ0 ura3Δ0*
BY4741 *MATa his3Δ1 leu2Δ0 met15Δ0 ura3Δ0 SNF1-GFP-HIS3MX NRD1-mCherry-Hph*
BY4741 *MATa his3Δ1 leu2Δ0 met15Δ0 ura3Δ0 ΔMig1::kanMX*
W303-1A (202) *MATa {leu2-3,112 trp1-1 can1-100 ura3-1 ade2-1 his3-11,15}*
W303-1A (202) *MATa {leu2-3,112 trp1-1 can1-100 ura3-1 ade2-1 his3-11,15} NRD1-mCherry- Hph MIG1-GFP-KanMX*
W303-1A (202) *MATa {leu2-3,112 trp1-1 can1-100 ura3-1 ade2-1 his3-11,15 Δ Snf1::KanM*

Plasmids used in this study:

Mig1-HA *URA3* pRS316 (Schmidt et al., 2020)
Snf1-HA *URA3* pMR2307 (McCartney and Schmidt, 2001)
*HXK1*p-Citrine(A206K) BamHIlinker *ADH1*tail-*ACT1*t (Schmidt et al., 2020)
*SUC2*p-Citrine(A206K) BamHIlinker *ADH1*tail-*ACT1*t (Schmidt et al., 2020)

Fluorescent Recovery After Photobleaching (FRAP)

BY4741 and BY4741 *SNF1-GFP-HIS3MX NRD1-mCherry-Hph* were grown in YNB to exponential phase, OD ≈ 0.3, and immobilized on an 8-well Chambered Coverglass (Ibidi) coated with poly-L-lysine (Sigma). Media was switched to YNB supplemented with Complete Supplement Mix (Formedium) with either 2% glucose, 0.05% glucose or 2% glycerol at least 1h before imaging to ensure adaptation to the new carbon source. At least 20 cells per condition were imaged on ELYRA PS.1 SIM/PAL-M LSM780 (Zeiss) using Plan-Apochromat 40x /1.4 oil immersion objective, with settings: 1.59 Airy which equals 1.1 µm z sectioning, 6X zoom with pixel size of 0.28µm and pixel dwell time of 6.14 sec. The cells were continuously imaged for 100 frames, and bleaching was done in 20 bursts at 25% after 10 pre-scans using a circular ROI, of 6 pixels in diameter covering the nucleus.

Image processing: The average fluorescent intensity was extracted from the time-lapse image series as well as the time index for each image using the ZEN software (Zeiss). Given the values for background intensity, the intensity for the nuclear region, as well as a control region containing adjacent cells in the same frame, background removal and bleaching correction was done in RStudio (RStudio Team, 2020), Version 1.4.1106 , and the intensities were normalized based on the pre-scans.

Non-linear mixed effect model: A non-linear mixed-effect regression method for analyzing FRAP data was implemented and simulated in Monolix (version 2020R1, Antony, France: Lixoft SAS, 2021 (Kuhn and Lavielle, 2005)). The data, project files and models are available at github repository: https://github.com/cvijoviclab/Mig1_frap_nlme.

We used both a double exponential and a single exponential function to fit the data:

Single exponential: $I = I_0 + A1 * (1 - e^{-tau1*t})$
Double exponential: $I = I_0 + A1 * (1 - e^{-tau1*t}) + A2 * (1 - e^{-tau2*t})$,

where I_0 represent the degree of bleaching, $A1$ is the mobility constant, and $tau1$ the kinetic constant.

When bleaching the nucleus, a substantial proportion of the fluorescent protein pool is

bleached, affecting the calculations of the immobile fraction. To correct for this, the area of the nucleus and the cell was extracted from 20 cells in 0.05% glucose with Fiji software (Schindelin et al., 2012). This was used to calculate cell and nuclear volumes that were assumed to have a spherical shape. The nuclear to cytosolic ratio was calculated based on 20 cells in respective conditions using Fiji for extracting average intensities and R to calculate the ratios by creating a bleaching curve, apply correction and perform linear regression on the time series data. The bleached volume is 2.438379 µm3 and covers the nucleus and assuming Snf1 is mostly vacuole excluded (Chan and Marshall, 2014), 8.32% of the cytosol. The immobile fraction derived from the fitted model was then recalculated, accounting for the proportion of the bleached protein pool.

Steady-state localization microscopy

BY4741 and BY4741 *SNF1-GFP-HIS3MX NRD1-mCherry-Hph* were grown in YNB (Formedium) at 30°C into exponential phase and immobilized on an 8-well Chambered Coverglass (Ibidi) coated with poly-L-lysine (Sigma). Media was switched to YNB with either 2% glucose, 0.05% glucose or 2% glycerol at least 1h before imaging to ensure adaptation to the new carbon source. At least 20 cells/condition were imaged on either ELYRA PS.1 SIM/PAL-M LSM780 (Zeiss) using Plan-Apochromat 40x /1.4 oil immersion objective or DMi8 (Leica) with Lumencor SOLA SE led light (Lumencor) and Leica DFC9000 GT sCMOS camera using HCX PL APO 40x/1.3 oil immersion objective.

Image processing: Cell segmentation, extraction of mean intensities and background removal was done in Fiji software and MATLAB _R2019b. Plots and statistical analysis was done using RStudio, Version 1.4.1106.

Statistics: As the dataset did not pass the Shapiro–Wilk test, a non-parametric equivalent of ANOVA was used, the Kruskal-Wallis test. For pairwise comparison, a Wilcox test with Bonferroni correction was performed. These statistical tests were done in RStudio, Version 1.4.1106.

Short-timescale microfluidics experiments

The yeast strains were transformed with GFP-KanMX and mCherry hphNT1 using standard methods for yeast genetics and transformation (Daniel Gietz and Woods, 2002). Yeast strains were grown to mid-log phase at 30◦C in YNB synthetic complete medium containing 1.7 g/l yeast nitrogen base, 5 g/l ammonium sulfate, 670 mg/l complete supplement mix; 10 mg/l adenine and supplied with 540 mM ethanol overnight. A glass-bottom petri dish (GWST-5030, WillCo Wells, UK) was treated with concanavalin A solution (1 mg/ml in 10mM TrisHCl-buffer, 100mM NaCl, adjusted to pH 8.0 using 5 M HCl) for 30 min at room temperature. The concanavalin A solution was removed, and the cell suspension was added and incubated for 5 min at 30◦C. Cells which did not adhere to the surface were removed by washing with YNB. Exposure of cells to different media conditions was performed using a BioPen system (Fluicell AB, Sweden). Experiments were performed on an inverted microscope Olympus cellR widefield microscope system, based on an inverted IX81 motorized microscope with a Xe light source (MT20) and a Hamamatsu C8484 CCD camera. Images were acquired using a U PlanS Apo 40x NA 0.95l objective. The filter cubes, light intensities and exposure time and light intensities for all imaging channels used were as following for GFP: excitation 472/30mm emission 520/35nm with an intensity of 20% for 350 ms. mCherry: excitation 560/40 nm, emission 630/75 nm with an intensity of 20% for 150 ms. The microscope and the microfluidic device were controlled using the Experiment Manager in the Xcellence software. The

temperature was set to 30°C. Three images with an axial distance of 0.8 µm were acquired in transmission and fluorescent channels. The acquisition time for one set of images at each time point was ≈15 s. Images were acquired at changing imaging intervals to reduce phototoxicity and bleaching while keeping appropriate timing to monitor changes in Mig1 localization. Time-lapse imaging was performed 3 times every 30 s until the media shift, followed by 15 times every 20 s, followed by 5 times every 120 s, adding up to an overall experiment time of 16 min. Brightfield images acquired above the focal plane were divided by images acquired below the focal plane using custom Matlab scripts. Division of images leads to the elimination of uneven illumination and enhances the diffraction pattern of cells. Segmentation was performed on the resulting images using CellX (Mayer et al., 2013). The Mig1-localization index was calculated from the CellX output as follows:

$$\text{Localization index} = (\text{Median fluorescence\_nuc} / \text{Median fluorescence\_cell}) - 1$$

Cells were tracked using custom MATLAB scripts using previously described methods (Ricicova et al., 2013).

Western Blot analysis

Mig1 downshifts: BY4741 with mig1Δ was transformed with a Mig1-HA plasmid. Yeast strains were grown to mid-log phase at 30◦C in YNB, with 4% glucose, BY4741 was used as control. 5 minutes after the switch of media containing glucose or fructose in concentrations ranging between 0.28 mM to 220 mM, respectively 0,005% to 4%, the cells were harvested through incubation in 2M NaOH and subsequent incubation in 50% trichloroacetic acid.

Snf1 and Mig1 upshifts: *Snf1Δ* was transformed with the centromeric plasmid pSnf1-HA, and *mig1Δ* was transformed with the centromeric plasmid pMIG1-HA. Cells were grown to mid-log phase at 30◦C in YNB; 10 mg/l adenine and 540 mM ethanol overnight. The cells were switched to YNB containing a final concentration of glucose, fructose or mannose ranging between 0.28 mM to 220 mM, respectively 0,005% to 4%. 5 minutes after the switch, cells were harvested through incubation in 2M NaOH and subsequent incubation in 50% trichloroacetic acid.

Cells were harvested by centrifugation, and 50 µg of protein were applied to gel electrophoresis as previously described (Bendrioua et al., 2014). The protein concentration was determined by the DC protein assay kit (Bio-Rad, Hercules). Proteins were detected using rabbit anti-phospho-Snf1 (1:1000, Santa Cruz Biotech) and mouse anti-HA (1:2000, Cell signaling technology) or (F-7)(1:1000, Santa Cruz Biotech) antibodies. Primary antibodies were detected simultaneously with goat anti-mouse IRDye-800CW (1:15,000, LI-COR Biosciences) and anti-rabbit IRDye-680CW (1:15,000, LI-COR Biosciences) or m-IgGκ BP-HRP (1:1000, Santa Cruz Biotech).

***HXK1* and *SUC2* gene expression measurement**

The yeast cells (W303) were transformed with either *HXK1p-Citrine-ACT1t* or *SUC2p-Citrine-ACT1t*. The transformed cells were grown overnight on 3% ethanol as described above. The media in the cell was exchanged by centrifugation and adding new media with the required carbon-source concentration. After 2 hours, imaging was performed on a Leica DMi8 inverted fluorescence microscope (Leica microsystems). The microscope was equipped with a HCX PL APO 40 × /1.30 oil objective (Leica microsystems), Lumencor SOLA SE (Lumencor) led light and Leica DFC9000 GT sCMOS camera (Leica

microsystems). Citrine expression was observed with an excitation: 500/20, dichroic: 515 and emission: 535/30 filter cube at 150ms. Analysis of fluorescence intensity was performed with the ImageJ distribution FIJI.

Discussion

In this work, we studied the spatial distribution of Snf1 under different glucose concentrations and the kinetics of the nucleocytoplasmic shuttling by employing a FRAP method. We found that both the spatial distribution of Snf1 and the kinetics of the nucleocytoplasmic shuttling have a steady-state equilibrium that depends to a greater extent on the type of carbon source rather than on the concentration of glucose, which is in contrast to the Snf1 target, Mig1. Using non-linear mixed-effect regression, a negative correlation between Snf1 mobility and the kinetic constant of the nucleocytoplasmic, shuttling was observed within the conditions, while a positive trend was observed between different conditions. This indicates that two different mechanisms are at play, including at least one negative feedback loop. Further, we showed that Mig1 localization correlates with the Snf1 phosphorylation pattern and not with the Mig1 phosphorylation pattern, suggesting that inactivation of Snf1 has a more pronounced effect on the localization of Mig1 than on the phosphorylation of Mig1. Previous studies showed a Snf1 dependent and independent dephosphorylation of Mig1 (Wollman et al., 2017). Together, this indicates that nuclear localization and dephosphorylation of Mig1 is not exclusively triggered through phosphorylation by Snf1. Our time-lapse fluorescent microscopy shows that the intensity of Mig1 localization differs between the same concentration of different hexose sugars in the first 15 minutes after the upshift. Thus, the Snf1/Mig1 pathway seems to be more sensitive to glucose than to fructose and mannose.

Our main observation indicates that Snf1 is more sensitive to the presence of glucose rather than the concentration of glucose. This is in contrast to Mig1, which reacts strongly to the glucose concentrations. When we measured the steady-state NC ratio of Snf1 and Mig1 after shifting glucose grown cells to 2% glucose, 0.05% glucose and 2% glycerol, we observed that Mig1 had a large difference in NC ratio between the low and the high glucose concentrations, while the NC ratio in 0.05% glucose and 2% glycerol was similar. The NC ratio of Snf1 does not change significantly between the two glucose concentrations but is significant when comparing the glucose condition to the 2% glycerol, where we also observe a higher cell-to-cell variability. These data are consistent with previous time-lapse studies on Mig1 where in glucose grown cells shifted to 2% glucose, Mig1 stayed nuclear after 2h. In cells moved to a concentration below 0.2% glucose, Mig1 shifted to the cytosol and remained cytosolic after 2h (Bendrioua et al., 2014). This is also consistent with the data on expression from the promotor of the glucose repressed genes *HXK1* and *SUC2*, where we observed expression in 0.05% glucose but not in 4% glucose. In 0% glucose, we expect expression as in the 0.05% glucose case, but we observed an expression level similar as in 4% glucose, indicating glucose repression. This can either be caused by the lack of building blocks for YFP due to the prolonged glucose starvation or a second regulatory system, which, after the transcription repression, is needed to activate the expression of *HXK1* and *SUC2* promotor. Still, this indicates that glucose de-repression is starting already at 0.05% glucose where the bulk Mig1 is located in the cytosol. Snf1 activity is necessary to mediate glucose de-repression, but interestingly Snf1 is showing a phosphorylation level at 0.05%, more similar to the levels at 4% glucose, strengthening the argument that Snf1 is more sensitive to the presence of glucose while Mig1 reacts to the concentration of glucose. However, Snf1 has been shown to be transiently phosphorylated after a shift to lower glucose levels indicating that Snf1 is also

somehow sensing concentrations of glucose (Bendrioua et al., 2014). Furthermore, in the parameters fitted from the FRAP recovery curves, the two glucose conditions behave similarly, while the larger difference is between glucose and glycerol.

We also observed that steady-state Mig1 localization could be correlated to glucose concentration. Moreover, we investigated the transient localization of Mig1 after a shift in glucose concentration. For glucose, we observed Mig1 localizing to the nucleus at 0.005% glucose, as reported previously (Bendrioua et al., 2014; Devit et al., 1997). For mannose and fructose, we observed Mig1 nuclear localization only at concentrations 0.05% and above. For all hexoses, the Mig1 nuclear intensity increased in a dose-dependent manner, however the rate of increase is hexose specific. It remains unclear whether this is caused due to a higher enzyme specificity to glucose or another reason.

From the parameters inferred by the FRAP recovery curves, a negative correlation between mobility (parameter $A1$) and the kinetic constant ($tau1$) has been observed, indicating the existence of a negative feedback loop. Previous studies suggest the presence of a feedback loop where the concentration of Snf1 inhibit the phosphorylation status of Snf1, and the phosphorylation status is in turn regulating the levels of Snf1 (Hsu et al., 2015). Furthermore, taken in the context where Snf1 needs to be phosphorylated in order to accumulate in the nucleus (Hedbacker et al., 2004), this can potentially be the negative feedback loop we observe in the FRAP data. One straightforward interpretation is that cells subjected to the same carbon source and concentration but with a large fraction of the Snf1 pool bound to other processes need a higher activity of the nucleocytoplasmic shuttling to serve the same function. Previous studies suggest that the levels and the phosphorylation status of Snf1 are reciprocally regulated, as hyperphosphorylation has been observed when the levels of Snf1 is lower than normal (Hsu et al., 2015). This would fit with a model where nucleocytoplasmic shuttling is regulated by Snf1 phosphorylation status. A lower amount of mobile Snf1 would lead to a higher degree of phosphorylation in the available Snf1 and an increase in nucleocytoplasmic shuttling.

This model would explain the negative feedback loop but not the positive trend between mobility and kinetics observed in this study when exposing the cells to different carbon sources or levels. The levels of Snf1 in cells grown in 2% glycerol compared to glucose grown cells are significantly lower. Both the levels and the fraction of phosphorylated Snf1 are similar in glucose grown cells, in contrast to glycerol grown cells, where higher phosphorylation in glycerol grown cells shows slower kinetics. Instead, other mechanisms might provide a better explanation. It is not known whether Snf1 mediates its own transport across the nuclear membrane. Nonetheless, it is suggested that Snf1 participates in the Mig1 repression complex but also that a fraction of Snf1 is present in the repression complex even at low glucose levels. The association of Snf1 to Mig1 repression complex is mediated through Hxk1 or Hxk2 and also contains Mig2, Reg1, Snf4 and Gal83 (Vega et al., 2016). However, this is not a 1:1 ratio as we see a large difference in nuclear intensity, and Mig1 operates in clusters (Wollman et al., 2017). Snf1 might also only participates in a fraction of the complexes formed by the Mig1 clusters. Either way, it is possible that Snf1 is co-localizing with other components of this complex and that they are regulating the nucleoplasm shuttling in regard to levels of glucose and type of carbon source. This is supported by the fact that Mig1 localization is affected by *hxk1/2*Δ and that this effect is different depending on both carbon source and level (Schmidt et al., 2020). The low phosphorylation levels of Snf1 in 0.05% glucose, the expression of glucose repressed genes and the overall low signal of Snf1 that are relatively evenly distributed in the cell with a relative high cell-to-cell variability in all conditions suggests that the role of Snf1

in the nucleus can be carried out by few numbers of proteins and the variability does not contribute significantly to Snf1 ability to perform its nuclear or cytoplasmic function.

Overall, these results, together with previous studies, suggest a two-step process of the Snf1 pathway that consists of localization and phosphorylation of the pathway components. One is phosphorylation-dependent and binary in its nature, the other is gradual and based on localization and mobility (Oh et al., 2020).

The Snf1/Mig1 pathway is immensely complex, and due to difficulties and lack of experimental methods for monitoring Snf1, the transcription factor Mig1 is often used as a readout. However, previous studies have pointed out that Mig1 is regulated both by a Snf1 dependent and a Snf1 independent mechanism, making it hard to infer the mechanistic behavior of Snf1 by monitoring Mig1. With this study, we can confirm that many aspects of Snf1 and Mig1 behave differently and contribute to the demarcation of the responses. To further elucidate the dynamics and mechanism of the Snf1 pathway, the development of tools for monitoring Snf1, preferably in single cells in yeast, would be needed. For example, a method for monitoring phosphorylation levels without the risk of activating Snf1 or a method to investigate the complexes that Snf1 participates in during different conditions.

In this work, we employed non-linear mixed effect regression to analyze FRAP data, enabling inference of more information than using traditional regression methods. We show that a negative feedback loop controls Snf1 nucleocytoplasmic shuttling. Further, we hypothesize that part of the Snf1 pathway functions as a switch, in which Snf1 is dephosphorylated once glucose is taken up by the cell, and part of the pathway functions as a slider which the level of activation depends on the concentration of hexose sugars. This gives the Snf1-Mig1 system the flexibility and sensitivity to fine-tune itself dynamically to the metabolic state of the cell.

Funding:
This work was supported by the Swedish Research Council (VR2016-03744 and VR2017-05117) and the Swedish Foundation for Strategic Research (FFL15-0238).

Acknowledgments:
We acknowledge the Cvijovic group members for input and support along the way. We acknowledge the Centre for Cellular Imaging at the University of Gothenburg for giving us access to high-resolution techniques and excellent guidance in the world of imaging.

Conflict of Interest:
None declared

References

Almquist, J., Bendrioua, L., Adiels, C.B., Goksör, M., Hohmann, S., Jirstrand, M., 2015. A Nonlinear Mixed Effects Approach for Modeling the Cell-To-Cell Variability of Mig1 Dynamics in Yeast. PLOS ONE 10, e0124050. https://doi.org/10.1371/journal.pone.0124050

Bendrioua, L., Smedh, M., Almquist, J., Cvijovic, M., Jirstrand, M., Goksör, M., Adiels, C.B., Hohmann, S., 2014. Yeast AMP-activated Protein Kinase Monitors Glucose Concentration Changes and Absolute Glucose Levels. Journal of Biological Chemistry 289, 12863–12875. https://doi.org/10.1074/jbc.m114.547976

574 Berthels, N.J., Cordero Otero, R.R., Bauer, F.F., Pretorius, I.S., Thevelein, J.M., 2008.
575 Correlation between glucose/fructose discrepancy and hexokinase kinetic properties
576 in different Saccharomyces cerevisiae wine yeast strains. Appl Microbiol Biotechnol
577 77, 1083–1091. https://doi.org/10.1007/s00253-007-1231-2
578 Carlson, M., Osmond, B.C., Botstein, D., 1981. MUTANTS OF YEAST DEFECTIVE IN
579 SUCROSE UTILIZATION. Genetics 98, 25–40.
580 https://doi.org/10.1093/genetics/98.1.25
581 Celenza, J.L., Eng, F.J., Carlson, M., 1989. Molecular analysis of the SNF4 gene of
582 Saccharomyces cerevisiae: evidence for physical association of the SNF4 protein with
583 the SNF1 protein kinase. Molecular and Cellular Biology 9, 5045–5054.
584 https://doi.org/10.1128/mcb.9.11.5045
585 Chan, Y.-H.M., Marshall, W.F., 2014. Organelle Size Scaling of the Budding Yeast Vacuole
586 Is Tuned by Membrane Trafficking Rates. Biophys J 106, 1986–1996.
587 https://doi.org/10.1016/j.bpj.2014.03.014
588 Chandrashekarappa, D.G., McCartney, R.R., O'Donnell, A.F., Schmidt, M.C., 2016. The β
589 subunit of yeast AMP-activated protein kinase directs substrate specificity in response
590 to alkaline stress. Cellular Signalling 28, 1881–1893.
591 https://doi.org/10.1016/j.cellsig.2016.08.016
592 Chandrashekarappa, D.G., McCartney, R.R., Schmidt, M.C., 2013. Ligand Binding to the
593 AMP-activated Protein Kinase Active Site Mediates Protection of the Activation
594 Loop from Dephosphorylation*,. Journal of Biological Chemistry 288, 89–98.
595 https://doi.org/10.1074/jbc.M112.422659
596 Daniel Gietz, R., Woods, R.A., 2002. Transformation of yeast by lithium acetate/single-
597 stranded carrier DNA/polyethylene glycol method. Guide to Yeast Genetics and
598 Molecular and Cell Biology - Part B 87–96. https://doi.org/10.1016/s0076-
599 6879(02)50957-5
600 Davidian, M., Giltinan, D.M., 2003. Nonlinear models for repeated measurement data: An
601 overview and update. JABES 8, 387–419. https://doi.org/10.1198/1085711032697
602 DeVit, M.J., Johnston, M., 1999. The nuclear exportin Msn5 is required for nuclear export of
603 the Mig1 glucose repressor of Saccharomyces cerevisiae. Current Biology 9, 1231–
604 1241. https://doi.org/10.1016/s0960-9822(99)80503-x
605 Devit, M.J., Waddle, J.A., Johnston, M., 1997. Regulated nuclear translocation of the Mig1
606 glucose repressor. Molecular Biology of the Cell 8, 1603–1618.
607 https://doi.org/10.1091/mbc.8.8.1603
608 Gancedo, J.M., 1998. Yeast carbon catabolite repression. Microbiol Mol Biol Rev 62, 334–
609 361. https://doi.org/10.1128/MMBR.62.2.334-361.1998
610 García-Salcedo, R., Lubitz, T., Beltran, G., Elbing, K., Tian, Y., Frey, S., Wolkenhauer, O.,
611 Krantz, M., Klipp, E., Hohmann, S., 2014. Glucose de-repression by yeast AMP-
612 activated protein kinase SNF1 is controlled via at least two independent steps. FEBS
613 Journal 281, 1901–1917. https://doi.org/10.1111/febs.12753
614 Hardie, D.G., 2014. AMPK—Sensing Energy while Talking to Other Signaling Pathways.
615 Cell Metabolism 20, 939–952. https://doi.org/10.1016/j.cmet.2014.09.013
616 Hardie, D.G., Ross, F.A., Hawley, S.A., 2012. AMP-Activated Protein Kinase: A Target for
617 Drugs both Ancient and Modern. Chemistry & Biology 19, 1222–1236.
618 https://doi.org/10.1016/j.chembiol.2012.08.019
619 Hedbacker, K., Carlson, M., 2008. SNF1/AMPK pathways in yeast. Frontiers in Bioscience
620 13, 2408. https://doi.org/10.2741/2854
621 Hedbacker, K., Hong, S.-P., Carlson, M., 2004. Pak1 Protein Kinase Regulates Activation
622 and Nuclear Localization of Snf1-Gal83 Protein Kinase. Molecular and Cellular
623 Biology 24, 8255–8263. https://doi.org/10.1128/mcb.24.18.8255-8263.2004

Hong, S.-P., Leiper, F.C., Woods, A., Carling, D., Carlson, M., 2003. Activation of yeast Snf1 and mammalian AMP-activated protein kinase by upstream kinases. Proceedings of the National Academy of Sciences 100, 8839–8843. https://doi.org/10.1073/pnas.1533136100

Hsu, H.E., Liu, T.N., Yeh, C.S., Chang, T.H., Lo, Y.C., Kao, C.F., 2015. Feedback control of Snf1 protein and its phosphorylation is necessary for adaptation to environmental stress. Journal of Biological Chemistry 290, 16786–16796. https://doi.org/10.1074/jbc.M115.639443

Jiang, R., Carlson, M., 1997. The Snf1 protein kinase and its activating subunit, Snf4, interact with distinct domains of the Sip1/Sip2/Gal83 component in the kinase complex. Molecular and Cellular Biology 17, 2099–2106. https://doi.org/10.1128/mcb.17.4.2099

Keleher, C.A., Redd, M.J., Schultz, J., Carlson, M., Johnson, A.D., 1992. Ssn6-Tup1 is a general repressor of transcription in yeast. Cell 68, 709–719. https://doi.org/10.1016/0092-8674(92)90146-4

Kuhn, E., Lavielle, M., 2005. Maximum likelihood estimation in nonlinear mixed effects models. Computational Statistics & Data Analysis 49, 1020–1038. https://doi.org/10.1016/j.csda.2004.07.002

Lavielle, M., Mentré, F., 2007. Estimation of Population Pharmacokinetic Parameters of Saquinavir in HIV Patients with the MONOLIX Software. J Pharmacokinet Pharmacodyn 34, 229–249. https://doi.org/10.1007/s10928-006-9043-z

Llamosi, A., Gonzalez-Vargas, A.M., Versari, C., Cinquemani, E., Ferrari-Trecate, G., Hersen, P., Batt, G., 2016. What Population Reveals about Individual Cell Identity: Single-Cell Parameter Estimation of Models of Gene Expression in Yeast. PLOS Computational Biology 12, e1004706. https://doi.org/10.1371/journal.pcbi.1004706

Lutfiyya, L.L., Iyer, V.R., DeRisi, J., DeVit, M.J., Brown, P.O., Johnston, M., 1998. Characterization of Three Related Glucose Repressors and Genes They Regulate in Saccharomyces cerevisiae. Genetics 150, 1377–1391. https://doi.org/10.1093/genetics/150.4.1377

Lutfiyya, L.L., Johnston, M., 1996. Two zinc-finger-containing repressors are responsible for glucose repression of SUC2 expression. Molecular and Cellular Biology 16, 4790–4797. https://doi.org/10.1128/mcb.16.9.4790

Mayer, C., Dimopoulos, S., Rudolf, F., Stelling, J., 2013. Using CellX to Quantify Intracellular Events, in: Current Protocols in Molecular Biology. John Wiley & Sons, Inc. https://doi.org/10.1002/0471142727.mb1422s101

Mayer, F.V., Heath, R., Underwood, E., Sanders, M.J., Carmena, D., McCartney, R.R., Leiper, F.C., Xiao, B., Jing, C., Walker, P.A., Haire, L.F., Ogrodowicz, R., Martin, S.R., Schmidt, M.C., Gamblin, S.J., Carling, D., 2011. ADP Regulates SNF1, the Saccharomyces cerevisiae Homolog of AMP-Activated Protein Kinase. Cell Metabolism 14, 707–714. https://doi.org/10.1016/j.cmet.2011.09.009

McCartney, R.R., Schmidt, M.C., 2001. Regulation of Snf1 Kinase: ACTIVATION REQUIRES PHOSPHORYLATION OF THREONINE 210 BY AN UPSTREAM KINASE AS WELL AS A DISTINCT STEP MEDIATED BY THE Snf4 SUBUNIT*. Journal of Biological Chemistry 276, 36460–36466. https://doi.org/10.1074/jbc.M104418200

Nath, N., McCartney, R.R., Schmidt, M.C., 2003. Yeast Pak1 Kinase Associates with and Activates Snf1. Molecular and Cellular Biology 23, 3909–3917. https://doi.org/10.1128/mcb.23.11.3909-3917.2003

Oh, S., Lee, J., Swanson, S.K., Florens, L., Washburn, M.P., Workman, J.L., 2020. Yeast Nuak1 phosphorylates histone H3 threonine 11 in low glucose stress by the

674 cooperation of AMPK and CK2 signaling. eLife 9, e64588.
675 https://doi.org/10.7554/eLife.64588
676 Ostling, J., Ronne, H., 1998. Negative control of the Mig1p repressor by Snf1p-dependent
677 phosphorylation in the absence of glucose. European Journal of Biochemistry 252,
678 162–168. https://doi.org/10.1046/j.1432-1327.1998.2520162.x
679 Persson, S., Welkenhuysen, N., Shashkova, S., Cvijovic, M., 2020. Fine-Tuning of Energy
680 Levels Regulates SUC2 via a SNF1-Dependent Feedback Loop. Front. Physiol. 11.
681 https://doi.org/10.3389/fphys.2020.00954
682 Ricicova, M., Hamidi, M., Quiring, A., Niemisto, A., Emberly, E., Hansen, C.L., 2013.
683 Dissecting genealogy and cell cycle as sources of cell-to-cell variability in MAPK
684 signaling using high-throughput lineage tracking. Proceedings of the National
685 Academy of Sciences 110, 11403–11408. https://doi.org/10.1073/pnas.1215850110
686 RStudio Team, 2020. RStudio: Integrated Development Environment for R. RStudio, PBC.,
687 Boston, MA.
688 Ruiz, A., Xu, X., Carlson, M., 2013. Ptc1 Protein Phosphatase 2C Contributes to Glucose
689 Regulation of SNF1/AMP-activated Protein Kinase (AMPK) in Saccharomyces
690 cerevisiae. Journal of Biological Chemistry 288, 31052–31058.
691 https://doi.org/10.1074/jbc.m113.503763
692 Ruiz, A., Xu, X., Carlson, M., 2011. Roles of two protein phosphatases, Reg1-Glc7 and Sit4,
693 and glycogen synthesis in regulation of SNF1 protein kinase. Proceedings of the
694 National Academy of Sciences 108, 6349–6354.
695 https://doi.org/10.1073/pnas.1102758108
696 Schindelin, J., Arganda-Carreras, I., Frise, E., Kaynig, V., Longair, M., Pietzsch, T.,
697 Preibisch, S., Rueden, C., Saalfeld, S., Schmid, B., Tinevez, J.-Y., White, D.J.,
698 Hartenstein, V., Eliceiri, K., Tomancak, P., Cardona, A., 2012. Fiji: an open-source
699 platform for biological-image analysis. Nat Methods 9, 676–682.
700 https://doi.org/10.1038/nmeth.2019
701 Schmidt, G.W., Welkenhuysen, N., Ye, T., Cvijovic, M., Hohmann, S., 2020. Mig1
702 localization exhibits biphasic behavior which is controlled by both metabolic and
703 regulatory roles of the sugar kinases. Molecular Genetics and Genomics 295, 1489–
704 1500. https://doi.org/10.1007/s00438-020-01715-4
705 Schmidt, M.C., McCartney, R.R., 2000. beta-subunits of Snf1 kinase are required for kinase
706 function and substrate definition. The EMBO Journal 19, 4936–4943.
707 https://doi.org/10.1093/emboj/19.18.4936
708 Sissoko, D., Laouenan, C., Folkesson, E., M'Lebing, A.-B., Beavogui, A.-H., Baize, S.,
709 Camara, A.-M., Maes, P., Shepherd, S., Danel, C., Carazo, S., Conde, M.N., Gala, J.-
710 L., Colin, G., Savini, H., Bore, J.A., Marcis, F.L., Koundouno, Fara Raymond,
711 Petitjean, F., Lamah, M.-C., Diederich, S., Tounkara, A., Poelart, G., Berbain, E.,
712 Dindart, J.-M., Duraffour, S., Lefevre, A., Leno, T., Peyrouset, O., Irenge, L.,
713 Bangoura, N., Palich, R., Hinzmann, J., Kraus, A., Barry, T.S., Berette, S., Bongono,
714 A., Camara, M.S., Munoz, V.C., Doumbouya, L., Harouna, S., Kighoma, P.M.,
715 Koundouno, Fara Roger, Lolamou, R., Loua, C.M., Massala, V., Moumouni, K.,
716 Provost, C., Samake, N., Sekou, C., Soumah, A., Arnould, I., Komano, M.S., Gustin,
717 L., Berutto, C., Camara, D., Camara, F.S., Colpaert, J., Delamou, L., Jansson, L.,
718 Kourouma, E., Loua, M., Malme, K., Manfrin, E., Maomou, A., Milinouno, A.,
719 Ombelet, S., Sidiboun, A.Y., Verreckt, I., Yombouno, P., Bocquin, A., Carbonnelle,
720 C., Carmoi, T., Frange, P., Mely, S., Nguyen, V.-K., Pannetier, D., Taburet, A.-M.,
721 Treluyer, J.-M., Kolie, J., Moh, R., Gonzalez, M.C., Kuisma, E., Liedigk, B., Ngabo,
722 D., Rudolf, M., Thom, R., Kerber, R., Gabriel, M., Caro, A.D., Wölfel, R., Badir, J.,
723 Bentahir, M., Deccache, Y., Dumont, C., Durant, J.-F., Bakkouri, K.E., Uwamahoro,

M.G., Smits, B., Toufik, N., Cauwenberghe, S.V., Ezzedine, K., Dortenzio, E., Pizarro, L., Etienne, A., Guedj, J., Fizet, A., Fare, E.B. de S., Murgue, B., Tran-Minh, T., Rapp, C., Piguet, P., Poncin, M., Draguez, B., Duverger, T.A., Barbe, S., Baret, G., Defourny, I., Carroll, M., Raoul, H., Augier, A., Eholie, S.P., Yazdanpanah, Y., Levy-Marchal, C., Antierrens, A., Herp, M.V., Günther, S., Lamballerie, X. de, Keïta, S., Mentre, F., Anglaret, X., Malvy, D., Group, J.S., 2016. Experimental Treatment with Favipiravir for Ebola Virus Disease (the JIKI Trial): A Historically Controlled, Single-Arm Proof-of-Concept Trial in Guinea. PLOS Medicine 13, e1001967. https://doi.org/10.1371/journal.pmed.1001967

Treitel, M.A., Carlson, M., 1995. Repression by SSN6-TUP1 is directed by MIG1, a repressor/activator protein. Proceedings of the National Academy of Sciences 92, 3132–3136. https://doi.org/10.1073/pnas.92.8.3132

Treitel, M.A., Kuchin, S., Carlson, M., 1998. Snf1 Protein Kinase Regulates Phosphorylation of the Mig1 Repressor in Saccharomyces cerevisiae. Molecular and Cellular Biology 18, 6273–6280. https://doi.org/10.1128/mcb.18.11.6273

Usaite, R., Jewett, M.C., Oliveira, A.P., Yates, J.R., Olsson, L., Nielsen, J., 2009. Reconstruction of the yeast Snf1 kinase regulatory network reveals its role as a global energy regulator. Molecular Systems Biology 5, 319. https://doi.org/10.1038/msb.2009.67

Vega, M., Riera, A., Fernández-Cid, A., Herrero, P., Moreno, F., 2016. Hexokinase 2 Is an Intracellular Glucose Sensor of Yeast Cells That Maintains the Structure and Activity of Mig1 Protein Repressor Complex *. https://doi.org/10.1074/jbc.M115.711408

Vincent, O., Townley, R., Kuchin, S., Carlson, M., 2001. Subcellular localization of the Snf1 kinase is regulated by specific beta subunits and a novel glucose signaling mechanism. Genes & development 15, 1104–14. https://doi.org/10.1101/gad.879301

Welkenhuysen, N., Borgqvist, J., Backman, M., Bendrioua, L., Goksör, M., Adiels, C.B., Cvijovic, M., Hohmann, S., 2017. Single-cell study links metabolism with nutrient signaling and reveals sources of variability. BMC Systems Biology 11. https://doi.org/10.1186/s12918-017-0435-z

Wollman, A.J.M., Shashkova, S., Hedlund, E.G., Friemann, R., Hohmann, S., Leake, M.C., 2017. Transcription factor clusters regulate genes in eukaryotic cells. eLife 6. https://doi.org/10.7554/eLife.27451

Ye, T., Elbing, K., Hohmann, S., 2008. The pathway by which the yeast protein kinase Snf1p controls acquisition of sodium tolerance is different from that mediating glucose regulation. Microbiology 154, 2814–2826. https://doi.org/10.1099/mic.0.2008/020149-0

Zhang, J., Olsson, L., Nielsen, J., 2010. The β-subunits of the Snf1 kinase in Saccharomyces cerevisiae, Gal83 and Sip2, but not Sip1, are redundant in glucose derepression and regulation of sterol biosynthesis. Molecular Microbiology 77, 371–383. https://doi.org/10.1111/j.1365-2958.2010.07209.x

Zhang, Y., McCartney, R.R., Chandrashekarappa, D.G., Mangat, S., Schmidt, M.C., 2011. Reg1 protein regulates phosphorylation of all three Snf1 isoforms but preferentially associates with the Gal83 isoform. Eukaryot Cell 10, 1628–1636. https://doi.org/10.1128/EC.05176-11